Journal of Power Sources 655 (2025) 237989

Contents lists available at ScienceDirect

Journal of Power Sources

journal homepage: www.elsevier.com/locate/jpowsour

Constructing efficient SPAN based energy storage batteries via the introduction of Cu_2S-Li_2S displacement reaction

Yi Deng [a], Qichen Chen [b], Jiaxiang Liu [a], Yuejing Zeng [b], Ruilai Ye [a], Xinyu Li [a], Peng Zhang [a,*], Jinbao Zhao [b,**]

[a] College of Energy & School of Energy Research, Xiamen University, Xiamen, 361102, PR China
[b] State Key Lab of Physical Chemistry of Solid Surfaces, State-Province Joint Engineering Laboratory of Power Source Technology for New Energy Vehicle, College of Chemistry and Chemical Engineering, Xiamen University, Xiamen, 361005, PR China

HIGHLIGHTS

- Displacement reaction was first used to optimize SPAN-based battery cycling.
- Cu_2S-driven strategy boosts kinetics and significantly reduces polarization.
- Cu-SPAN/CNT demonstrates an excellent energy utilization efficiency of 79.8 %.

GRAPHICAL ABSTRACT

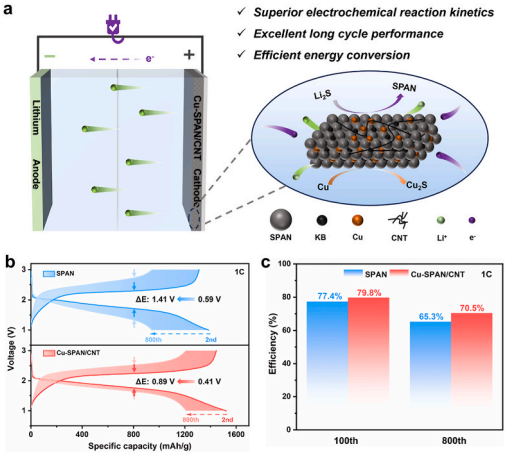

ARTICLE INFO

Keywords:
Sulfurized polyacrylonitrile
Copper-polysulphide reaction
Reaction kinetics
Energy storage battery
Lithium sulfur battery

ABSTRACT

Sulfurized polyacrylonitrile (SPAN), as an inherently safe, low-cost, and long-cycle-life material, holds a promising future in large-scale energy storage applications. However, there are still issues such as sluggish electrochemical reaction kinetics and low energy utilization efficiency, which severely constrain practical applications. Herein, we introduce the displacement reaction of Cu_2S-Li_2S to the conversion reaction of SPAN/Li_2S by incorporating Carbon Nanotube (CNT) and Copper (Cu) to fabricate Cu-SPAN/CNT cathode. Detailed experimental investigations demonstrate the fast and reversible Cu_2S-Li_2S displacement reaction, enhancing the SPAN/Li_2S redox kinetics. Consequently, Cu-SPAN/CNT achieves 1450 mAh g^{-1} at 1 C with 80.3 % retention after 1000 cycles, while delivering 1207 mAh g^{-1} at 4 C and maintaining operation under practical conditions (6.75 mg cm^{-2} sulfur loading, −20 °C). Crucially, it attains 79.8 % energy utilization efficiency at the 100th cycle. In conclusion, this work optimizes the cycling process of SPAN-based batteries, particularly the highly

* Corresponding author.
** Corresponding author.
E-mail addresses: pengzhang@xmu.edu.cn (P. Zhang), jbzhao@xmu.edu.cn (J. Zhao).

https://doi.org/10.1016/j.jpowsour.2025.237989
Received 14 April 2025; Received in revised form 7 July 2025; Accepted 25 July 2025
Available online 29 July 2025

polarized charging processes, providing a simple solution for developing energy storage applications with extended cycle life, accelerated reaction kinetics, and enhanced energy utilization efficiency.

1. Introduction

With growing demands for cost-efficient storage, the imperative to develop cost-effective, high-energy-density, long-cycle-life, and high-energy-efficiency storage batteries has become increasingly critical [1,2]. Lithium-sulfur battery (Li-S), owing to its high theoretical energy density of 2600 Wh kg^{-1} and the advantages of low cost, high abundance, and environmental friendliness of sulfur, is considered as one of the most promising candidates for the next generation of energy storage batteries [3,4]. However, the severe polysulfide shuttle effect and poor electrochemical reaction kinetics limit the widespread use of traditional Li-S batteries [5,6]. Sulfurized polyacrylonitrile (SPAN), as an inherently safe organic sulfur material, has been widely validated for its stable long-cycle performance, and its low-cost advantage aids in the advancement of large-scale energy storage systems [7,8]. Nonetheless, SPAN suffers from poor conductivity and high energy barriers for the electrochemical reaction of discharge product Li_2S [9,10]; simultaneously, its "solid-solid" conversion mechanism during the cycling processes results in high potential hysteresis [1,11,12]. This is manifested as larger polarization voltages, overcoming which requires the consumption of more energy, reducing the energy utilization efficiency of large-scale energy storage batteries, contradicting the goal of promoting efficient energy storage[13–15].

In past research, much attention has been focused on aspects such as the cycle life and discharge capacity of batteries, while the kinetically hindered charging process remains understudied. Optimizing charging behavior is critical for enhancing energy efficiency, as it directly correlates with electrochemical kinetics acceleration. In efforts to ameliorate the sluggish electrochemical reaction kinetics of SPAN, researchers have conducted regulatory optimizations from several aspects, including the compounding of conductive agents [16–19], doping with heteroatoms [1,20–22], the use of redox electrolyte additives [11,12,23,24], and improvements in electrode preparation processes [19,25–27]. These strategies are crucial for enhancing the performance of SPAN-based energy storage systems and are in line with the ongoing advancements in battery technology research. For instance, Wang et al. introduced carbon materials with superior conductivity, such as CNT [16], CNF [18], and rGO [28], into the PAN precursor to enhance the electronic conductivity of SPAN and Li_2S. Xie and Zuo et al. introduced non-metal elements such as selenium (Se) [1], tellurium (Te) [20], iodine (I) [21], and phosphorus (P) [22] from groups VA, VIA, and VIIA into the SPAN synthesis process to modify the material, thereby promoting electron and Li^+ migration and enhancing the electrochemical reaction kinetics. Wang et al. improved the cycling stability of SPAN in ether-based electrolytes and strengthened the reaction kinetics by adding small amounts of redox additives such as Li_2S_8 [23], phenyl diselenide (PDSe) [24], lithium selenide (Li_2Se) [11], and fluorinated anthraquinone (DFAQ) [14] to the electrolyte. Zhang et al.[29–32] employed methods such as electrospinning to mix CNT, Se with PAN (polyacrylonitrile) etc., to enhance the electrochemical reaction kinetics of SPAN from the aspects of catalytic activity and structural stability enhancement. Previous studies have predominantly focused on the modification of SPAN raw materials, doping with elements, and electrolyte additives. Nevertheless, the research on Li_2S during the charging process back to SPAN is relatively insufficient, while the high reaction energy barrier of Li_2S leads to a wide voltage hysteresis gap [33,34], ultimately resulting in a low charge-discharge energy efficiency. Reducing the activation potential of Li_2S and enhancing the stability of SPAN/Li_2S cycling constitutes a problem that urgently needs to be addressed.

Cu_2S shares structural similarities with Li_2S, and the ionic radii of Cu^+ and Li^+ are close (0.077 nm and 0.076 nm, respectively), with high ion diffusion coefficients (approximately 10^{-7} to 10^{-9} cm^2 s^{-1})[35–37]. This allows for a rapid and reversible displacement reaction between Cu^+ and Li^+ in the sulfur matrix, which effectively reduces the activation potential of Li_2S, enhancing its electrochemical activity and aiding in the optimization of the charging process [38]. Pioneering work by Tarascon (2006) [35] conducted research on the reaction mechanism of Cu with S and pointed out that the reaction between Cu_xS and Li_2S was a displacement reaction. Zhao et al. (2020) [37]significantly improved sulfur utilization and rate performance by adding Cu into the traditional sulfur cathode to introduce the displacement reaction. Subsequently, Guo et al. [38] found that incorporating Cu into the Li_2S cathode was helpful in reducing the activation potential of Li_2S and promoting the improvement of reaction kinetics. Consequently, introducing the displacement reaction involving Cu/Cu_2S into SPAN battery can not only improve the electronic conductivity of SPAN but also accelerate its sluggish solid-solid conversion process, especially the rate-determining step reaction of Li_2S. Moreover, enhancing the charge-discharge energy utilization efficiency of SPAN battery, which is of great significance for promoting the application of SPAN battery in large-scale energy storage.

In this work, the displacement reaction of Cu_2S-Li_2S is firstly introduced to the conventional conversion reaction of SPAN/Li_2S by a simple incorporating CNT and Cu strategy (Cu-SPAN/CNT). Electrochemical tests, including direct current polarization and cyclic voltammetry, confirmed the superior electronic and ionic conductivity of Cu-SPAN/CNT. Additionally, *in situ* XRD and XPS, combined with TEM characterization, have confirmed the rapid and reversible displacement reaction of Cu_2S-Li_2S, which accelerates the conversion between SPAN/Li_2S, improves the electrochemical reaction kinetics, and reduces the polarization voltage during the charge-discharge process. Consequently, Cu-SPAN/CNT exhibits enhanced long-term cycling stability, excellent high-rate performance, high-loading capacity, low-temperature performance and high energy utilization efficiency. Specifically, after 1000 cycles at 1 C, it retains a capacity of 80.3 %, with an average decay rate of merely 0.0197 % per cycle. At a high rate of 4 C, it delivers a high capacity of 1207 mAh g^{-1}, and it demonstrates outstanding performance under high sulfur loading of 6.75 mg cm^{-2} and at low temperatures of −20 °C. At the 100th cycle of 1 C, the Cu-SPAN/CNT demonstrates an excellent energy utilization efficiency of 79.8 % and reduced energy loss, which is equally important for large-scale energy storage. In summary, this work optimizes the charge-discharge process of SPAN-based batteries, particularly the highly polarized charging process, providing a scalable approach to achieve high-energy-density batteries with extended cycle life and improved energy efficiency.

2. Experimental section

2.1. Synthesis and preparation of materials

SPAN was synthesized by a co-heating method. Initially, 1 g of PAN (M_w 150000, Aldrich) was mixed with 4 g of sublimed sulfur (S_8, Aladdin). To facilitate dispersion, 10 mL of isopropanol was added as a dispersing agent. The mixture was ball-milled at a speed of 300 rpm for 6 h to ensure thorough mixing, then dried in a vacuum oven at 60 °C for 12 h. Subsequently, the sample was calcined in a ceramic boat under an argon atmosphere at 350 °C for 6 h [39,40]. After grinding, SPAN powder was obtained. Elemental analysis determined a sulfur content of 44.14 wt%.

The electrolyte was 1 M $LiPF_6$ dissolved in ethylene carbonate/diethyl carbonate (EC: DEC, volume ratio = 1:1), supplemented with 10 wt% fluoroethylene carbonate (FEC) obtained from DoDoChem. The

adding amount of electrolyte in coin cell is controlled at 100 μL, corresponding to an electrolyte-to-sulfur ratio (E/S) of approximately 88 μL mg^{-1}. The separator was 16 μm polyethylene (PE). Nano copper dispersed in ethylene glycol was subjected to vortex mixing followed by ultrasonication to ensure uniform dispersion prior to use. Conductive carbon black, Ketjenblack (KB), was procured from Suzhou Yilongsheng Energy Technology Co., Ltd. CNT (≥95 %, ID: 2–7 nm, OD: 11 nm, Length: 10 μm, Macklin). No further purification of the materials was conducted.

2.2. Preparation of Cu-SPAN/CNT and SPAN cathodes

Cu-SPAN/CNT Cathodes: A mixture of SPAN, KB, and CNT in a weight ratio of 80:5:5 was thoroughly ground, to which a binder 10 wt% LA133 was added. An appropriate amount of deionized water was used as a dispersant. The slurry was stirred at 2000 rpm for 15 min, after which a nano copper paste with a solid content of 5 wt% was added to the stirring box; the mixture was further stirred at 2000 rpm for an additional 15 min to ensure thorough mixing of Cu with SPAN, KB, and CNT. The slurry was then coated onto carbon-coated aluminum foil, pre-dried on a 60 °C heating plate, and subsequently transferred to a vacuum oven at 60 °C for overnight drying. The dried cathodes were punched into 12 mm diameter discs for later use, with a SPAN loading of approximately 3 mg cm^{-2}, equivalent to a sulfur loading of about 1.0–1.2 mg cm^{-2}.

SPAN Cathodes: The weight ratio of SPAN to KB was controlled at 80:10 wt%. following the same procedures as described above, with the sulfur loading controlled at approximately 1.0–1.2 mg cm^{-2}.

2.3. Material characterization

Elemental analysis for C, H, N, O, and S was conducted using an Elementar Unicube (CHNS/O) analyzer. The morphology of the samples was characterized by using a scanning electron microscope (SEM, TESCAN VEGA 3) and a transmission electron microscope (TEM, JEOL JEM-F200), with energy-dispersive X-ray spectroscopy (EDS, Oxford AZTECONE) employed for morphological and elemental distribution analysis. Additional TEM (Tecnai F30 TWIN, FEI) was utilized for morphological and elemental distribution assessment. Crystalline structure information was obtained using an X-ray diffractometer (Rigaku, Miniflex 600). Fourier-transform infrared spectroscopy (FT-IR, Bruker Vertex 70V) and Raman spectroscopy (LabRAM Odyssey with a 532 nm laser wavelength) were used to characterize the functional groups of SPAN. X-ray photoelectron spectroscopy (XPS, Thermo Scientific K-Alpha) was employed to analyze the transformation of sulfur-containing bonds in Cu-SPAN/CNT. *In situ* X-ray diffraction (*in situ* XRD) was performed using a Malvern Panalytical Empyrean system with X-ray radiation of wavelength 1.5406 Å (Cu Kα) to acquire *in situ* XRD patterns, aiding in the analysis of the mechanism of action of Cu within the battery.

2.4. Electrochemical measurement methods

Electrochemical performance of the materials was assessed using CR 2016 coin cells assembled in an argon-filled glovebox (O_2 < 0.05 ppm, H_2O < 0.05 ppm). The LAND battery tester was utilized for constant current charge-discharge tests at room temperature (25 °C), and the calculation of specific capacity is based on the sulfur mass in the cathode. Cyclic voltammetry (CV) tests were conducted using a Shanghai Chenhua CHI 660E electrochemical workstation, with a voltage range of 1–3 V and a scan rate of 0.1 mV s^{-1}. *In situ* electrochemical impedance spectroscopy (*in situ* EIS), variable scan rate cyclic voltammetry (diff-scan rate CV), and direct current polarization (DCP) tests were performed using a Swiss Metrohm AutoLab workstation. The amplitude for *in situ* impedance tests was 10 mV, with a frequency range from 10^5 Hz to 0.1 Hz; the diff-scan rate CV tests had a voltage range of 1–3 V with scan rates of 0.2, 0.4, 0.6, 0.8, and 1 mV s^{-1}; DC polarization tests were conducted using a symmetric cell with a stainless-steel disk structure to assess the electronic conductivity of the materials. Before DC polarization measurements, the prepared cathode powder was pressed into a disc with a diameter of 13 mm and a thickness of approximately 400 μm. Galvanostatic intermittent titration tests (GITT) were performed using a LAND battery tester, with conditions set for 120 min of charge-discharge followed by a 20-min pause.

3. Results and discussion

SPAN was synthesized via the method by ball milling S_8 with PAN and then co-heating them in Ar. Then, SPAN was mixed and stirred with KB and CNT, and 5 wt% Cu was added to prepare Cu-SPAN/CNT cathodes, as illustrated in the preparation process diagram (Fig. 1a). SEM was employed to observe the micromorphology of SPAN particles and the electrode before or after cycling, and Energy Dispersive Spectrometer (EDS) was used to characterize the elemental distribution. The morphology of SPAN, as shown in Fig. 1b, presents densely packed nanosphere-like particles, with individual particle sizes around 200–300 nm. Elemental analysis tests revealed that the mass content of S is 44.14 wt% (Table S1). As shown in Fig. S1, it is clearly visible that SPAN, KB, CNT, and Cu are uniformly distributed and intertwined, maintaining their connectivity even after cycling.

TEM was employed at a higher magnification, it can be observed that CNT act as a long-range conductive “bridge” connecting SPAN with KB and other particles (Fig. 1c–d), constructing an effective electronic conductive network that facilitates rapid electron transfer in the cathode. Simultaneously, along with corresponding elemental mapping images, reveal that uncycled SPAN particles exhibit an amorphous structure with uniform distribution of components (Fig. S2). Focusing on the Cu-SPAN/CNT, TEM images and elemental mapping reveal the uniform distribution of C, N, S, and Cu elements, indicating that nano Cu particles are well dispersed and can infiltrate the conductive network constructed by CNT and KB, maintaining close contact with SPAN particles, which contributes to leveraging the high energy density of SPAN (Fig. 1g–k). The uniform distribution of these elements indicates the effective integration of Cu within the electrode structure, facilitating the introduction of the Cu_2S displacement reaction during battery cycling. Furthermore, the high-resolution TEM tests were carried out on Cu-SPAN/CNT cathode of cycled (Fig. 1e–f). Obvious lattice fringes emerged on the amorphous SPAN particles, and the measured width was 0.326 nm, which corresponded to the (102) crystal plane of Cu_2S [38]. It is thus indicated that Cu plays a part in the reaction throughout the battery cycling, with a conversion from Cu to Cu_2S and an existence as Cu^+, persistently participating in the SPAN redox reactions.

The phase structure of the material was investigated by XRD patterns (Fig. 2a). Upon the addition of nano Cu, the Cu-SPAN/CNT cathode exhibited typical diffraction peaks at 43.3° (111) and 50.4° (200) corresponding to Cu (PDF# 085–1326). These peaks are clearly discernible, and no additional peaks for copper compounds such as Cu_xS or Cu_xO were observed, indicating that oxidation or sulfidation did not occur during the electrode preparation process. A broad diffraction peak around 25° was consistently observed across all cathodes, corresponding to the amorphous graphite/π-conjugated structure inherent in SPAN [21]. This observation suggests that the incorporation of CNT and Cu does not disrupt the amorphous carbon framework of SPAN. Fourier Transform Infrared Spectroscopy (FTIR), and Raman spectroscopy were employed to analyze the molecular and functional group structural information of the materials. The peaks at 668, 1240 and 1497 cm^{-1} are attributed to the stretching vibrations of the C-S, -C=N- and -C=C- bonds, respectively. The ring-breathing mode of the hexahydric-ring is observed at about 799 cm^{-1}, and the ring-breathing peak corresponding to the -C-S- bond appears at 940 cm^{-1} [1](Fig. 2b). As shown by the Raman spectroscopy, peaks at 308 and 369 cm^{-1} can be observed corresponding to C-S bonds, and peaks at 476 and 938 cm corresponding to S-S bonds are presented [13](Fig. 2c). No information regarding Cu-S

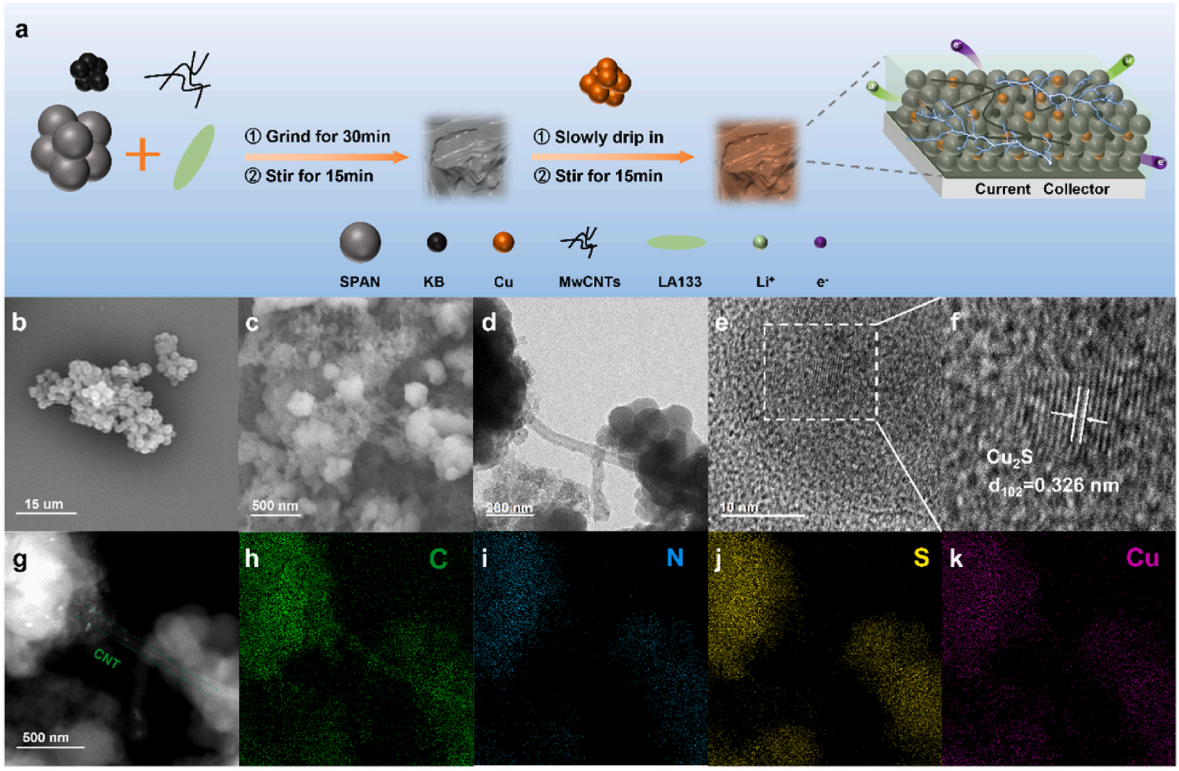

Fig. 1. (a) Schematic diagram of Cu-SPAN/CNT cathode preparation, (b) SEM image of SPAN, (c, d) TEM image of Cu-SPAN/CNT cathode, (e, f) TEM images of Cu-SPAN/CNT and Cu_2S lattice stripe, (g–k) TEM images of Cu-SPAN/CNT and elemental mapping of Cu-SPAN/CNT for carbon (C, green dots), nitrogen (N, blue dots), sulfur (S, yellow dots), and Copper (Cu, purple dots). (For interpretation of the references to color in this figure legend, the reader is referred to the Web version of this article.)

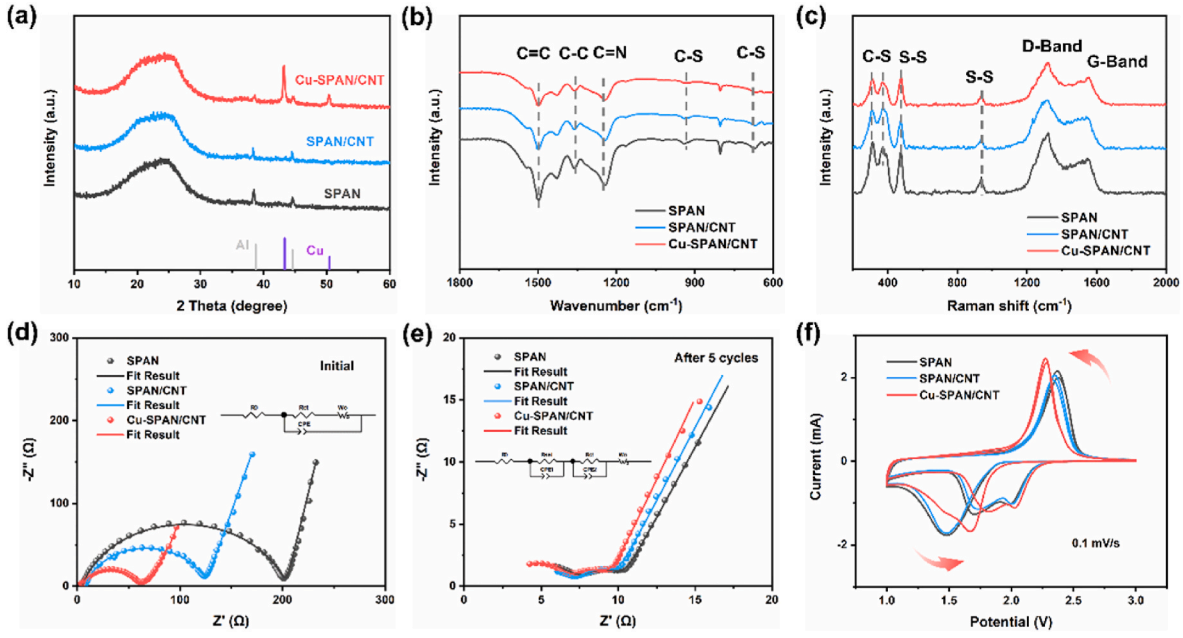

Fig. 2. (a) XRD patterns, (b) FT-IR spectra and (c) Raman spectra of SPAN, SPAN/CNT and Cu-SPAN/CNT cathodes. (d) Nyquist plots of initial and (e) after five cycles, (f) CV curves of SPAN, SPAN/CNT and Cu-SPAN/CNT batteries.

bonds was detected, and the molecular structure of SPAN remains intact. This indicates that the addition of CNT and Cu doesn't disrupt the SPAN structure, and it maintains its stability.

To investigate the reaction kinetics and interfacial structural changes of the electrode, EIS tests were conducted on different cathodes (Fig. 2d–e). At the initial stage, the impedance of Cu-SPAN/CNT was lower than that of SPAN/CNT, while the impedance of the unmodified SPAN cathode was the highest. This situation remained the same after 5 cycles. This suggests that the addition of CNT and Cu to the SPAN cathode enhanced electronic and Li^+ conduction, effectively reducing

ohmic resistance (R_0) and charge transfer resistance (R_{CT}), particularly at the initial, a pronounced discrepancy is evident (Table S2). Moreover, after 5 cycles, the Cu-SPAN/CNT maintains a substantially lower R_{CT} and solid electrolyte interphase resistance (R_{SEI}), facilitating rapid Li^+ diffusion across the electrode-electrolyte interface (Table S3). CV curves were conducted on the batteries with different cathodes (Fig. 2f). After adding CNT, thanks to the enhanced electronic conductivity, the intensity of the redox peak currents in the SPAN/CNT battery witnessed a slight increase, and the potential gap between oxidation and reduction was decreased. Subsequently, when Cu was added to the SPAN/CNT, the initial reduction peak current potentials of the SPAN and SPAN/CNT electrodes were observed to be within the range of 1.48–1.50 V. In contrast, those of the Cu-SPAN/CNT were around 1.70 V, indicating an elevation of approximately 0.20 V in the reduction potential. Therefore, compared with the improvement of electron conductivity by CNT, it is evident that the introduced displacement reaction is more effective in enhancing the reaction reversibility of SPAN. This shift is indicative of a higher discharge platform and enhanced cathodic reduction reaction kinetics, which is conducive to leveraging the high-capacity advantage of SPAN. At second cycle, the reduction peak potentials for the SPAN stabilized at around 1.75 V and 2.05 V, with Cu-SPAN/CNT showing an increase of about 0.1 V. Focusing on the oxidation process, the peak current of the Cu-SPAN/CNT is significantly sharper and the potential is lower, indicating that the incorporation of Cu can lower the activation potential of Li_2S. Consequently, the addition of CNT and Cu effectively improves the electrochemical reaction kinetics of SPAN, resulting in better reversibility of the reactions.

To validate the improvement in electronic transport properties of the modified cathode, DCP tests [21] were conducted on SPAN and Cu-SPAN/CNT electrodes (Fig. 3a), with the calculation method detailed in Equation (1). The calculated electronic conductivity of SPAN was found to be 8.59×10^{-5} S cm^{-1}, while that of Cu-SPAN/CNT was 9.46×10^{-5} S cm^{-1}, significantly higher than that of SPAN (Table S4). *In situ* EIS tests were conducted to investigate the continuous changes in the electrochemical reaction kinetics and interfacial structural evolution of the cathodes (Fig. 3b–c). During the discharge-charge process, the R_0 of Cu-SPAN/CNT at various state of charge (SOC) and depth of discharge (DOD) was consistently lower than that of SPAN. It is well known that R_0 is typically associated with the internal resistance of the electrode material, the contact resistance between the current collector and the electrode material. The smaller R_0 indicates that the incorporation of CNT and Cu has enhanced the overall electrical conductivity of the cathode, effectively reducing the internal resistance. Additionally, the R_{CT} of the Cu-SPAN/CNT remains consistently lower than that of the SPAN, and it further decreases with ongoing cycling. This reduction in R_{CT} for both systems is partly attributed to the improved electrical conductivity of SPAN because of the interaction between Li^+ and SPAN during the initial discharge [10]. Concurrently, the addition of CNT and Cu enhances the electrochemical properties of the cathode by increasing the active sites available for Li^+ transport, which in turn reduces R_{CT} and accelerates the electrochemical reaction kinetics.

Through GITT tests, the polarization voltage and charge transfer characteristics of different cathodes were examined. Compared to the SPAN, the Cu-SPAN/CNT exhibited a smaller voltage hysteresis gap during cycling, and the potential gap between the polarization potential and the quasi-equilibrium potential was reduced (Fig. S3). This indicates

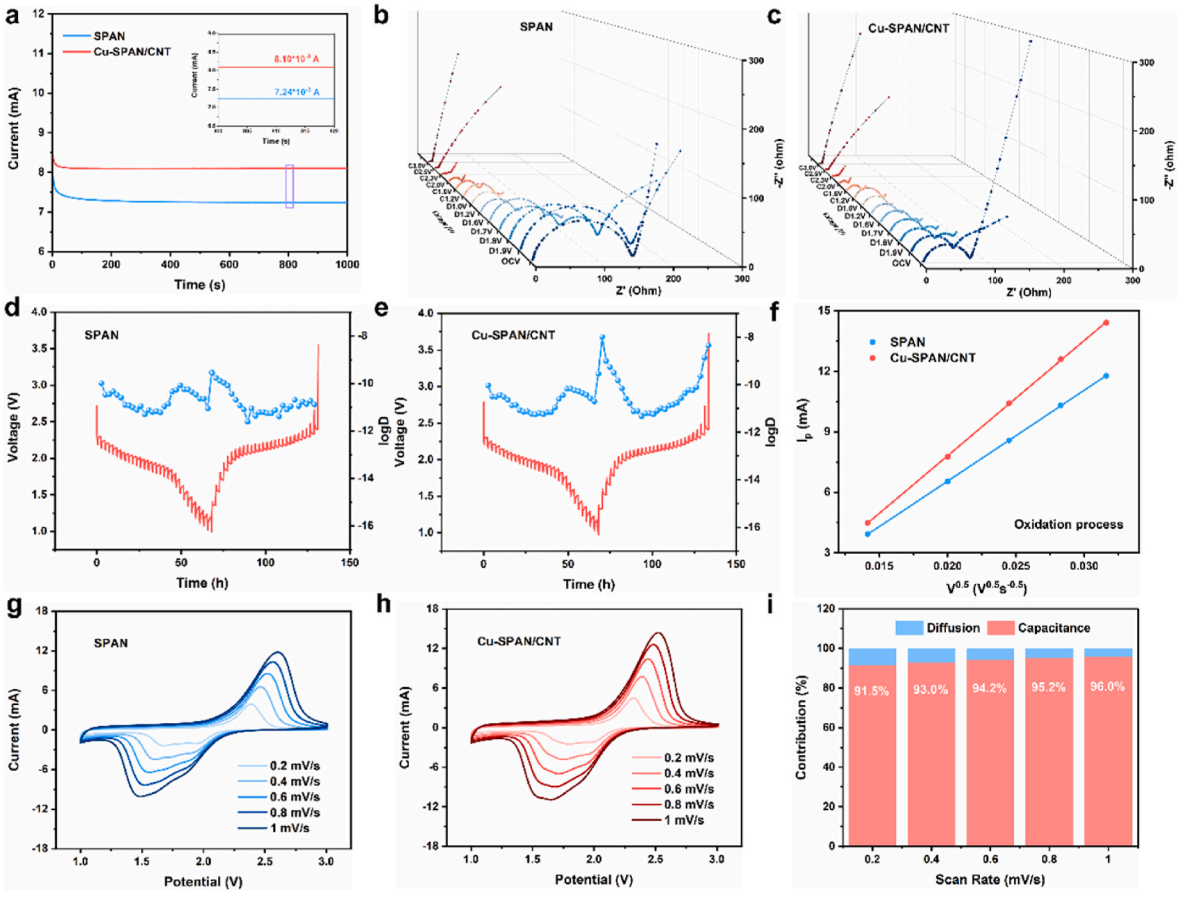

Fig. 3. (a) I-t curves of cathodes through DCP test. (b, c) *in situ* EIS measurement evolution of SPAN and Cu-SPAN/CNT. (d–e) The GITT profiles and Li^+ diffusion coefficients of SPAN and Cu-SPAN/CNT. (f) The peak currents versus square root of scan rates of SPAN and Cu-SPAN/CNT cathodes during oxidation process. (g–h) CV curves obtained at various scan rates of SPAN and Cu-SPAN/CNT. (i) Normalized contribution ratios of capacity/diffusion contribution at various scan rates of Cu-SPAN/CNT.

that the lithiation and delithiation kinetics of SPAN are faster, which is conducive to fully leveraging the high specific capacity of SPAN. Additionally, the GITT curves were utilized to calculate and compare the Li^+ diffusion coefficients, with Cu-SPAN/CNT demonstrating a higher diffusion coefficient, particularly evident during the charging process (Fig. 3d–e). More specifically, at early charging phase (1.0–1.5 V), corresponding to initial Li_2S decomposition, which occurred by slow kinetics. In conventional SPAN, substantial polarization occurs during initial charging, making Li^+ extraction from Li_2S difficult, resulting in low D_{Li}^+. For Cu-SPAN/CNT, the introduced Cu_2S displacement reaction effectively accelerates Li_2S decomposition, reduces the reaction energy barrier in early charging stages, and promotes Li^+ transport/migration, thereby significantly increasing D_{Li}^+ [38]. At late charging phase (2.5–3.0 V), corresponding to the delithiation-induced reconstruction phase of SPAN, most Li^+ ions have been extracted, while the residual Li^+ ions exhibit kinetic barriers during extraction [26]. In Cu-SPAN/CNT, the enhanced electronic/ionic conductivity of Cu/Cu_2S provides critical advantages. Even during late charging stages, this facilitates efficient Li^+/electron exchange in Cu-SPAN/CNT, effectively increasing D_{Li}^+. Therefore, the enhanced diffusion coefficient is a prerequisite for its higher sulfur utilization efficiency, excellent C-rate performance, and high energy utilization efficiency.

The CV curves tested by a range of scan rates were utilized to investigate the lithium-ion migration characteristics (Fig. 3g–h), the redox peak potential separation (ΔE_p) of Cu-SPAN/CNT was consistently smaller than that of SPAN across varying scan rates, indicating enhanced electrochemical reversibility, which is attributed to the synergistic suppression of polarization mechanisms. The continuous conductive network formed by CNT additives effectively reduces ohmic polarization (as verified by DC polarization analysis), while the Cu_2S-Li_2S displacement reaction mitigates electrochemical polarization by lowering the Li_2S decomposition energy barrier and enhancing Li^+ diffusion kinetics, which is supported by the reduced R_{CT} observed in EIS measurements. The optimized electronic/ionic conductivity of Cu-SPAN/CNT not only ensures reversible redox reactions but also enhances long-term cycling stability.

The apparent Li^+ diffusion coefficient (D_{Li}^+) was calculated according to the Randles-Sevick equation. At various scan rates, the peak currents of both oxidation and reduction for Cu-SPAN/CNT were higher than those of the SPAN, with a more pronounced difference observed during the oxidation process (Fig. 3f, Fig. S4a). This indicates that the incorporation of CNT and Cu significantly enhances the diffusion of Li^+ and improves the electrochemical reaction kinetics of SPAN. The Cu-SPAN/CNT exhibited a diffusion coefficient of 4.414×10^{-7} cm^2 s^{-1}, markedly higher than that of SPAN at 2.748×10^{-7} cm^2 s^{-1} (Fig. S4c). Furthermore, a fitting calculation was performed to analyze the capacity contribution. Typically, capacity contribution analysis to classify the total capacity into diffusion-limited reactions (DLR) and surface-driven processes (SDP) [41]. In which, SDP represents the rapid electrochemical reactions, and a higher proportion of SDP indicates superior charge and discharge capabilities of the battery. At various scan rates from 0.2 to 1.0 mV s^{-1}, the SDP contribution of Cu-SPAN/CNT was calculated to be 91.5 %, 93.0 %, 94.2 %, 95.2 %, and 96.0 %, respectively, which is significantly higher than that of SPAN (Fig. 3i, Fig. S4b). The detailed experimental results demonstrate that Cu-SPAN/CNT remarkably promotes the diffusion of Li^+, which is thanks to the rapid displacement reaction of Cu/Cu_2S, thereby resulting in faster electrochemical reaction kinetics.

To assess the role of the introduction of displacement reaction of Cu_2S-Li_2S, electrochemical performance tests were conducted on SPAN and Cu-SPAN/CNT. In the initial cycle, Cu-SPAN/CNT exhibited an impressive initial Coulombic efficiency of 80.2 %, demonstrating high sulfur utilization (Fig. S5). Assembled with Cu-SPAN/CNT as the cathode and lithium metal as the anode, a visually transparent cell [29] as depicted in Fig. S6a was constructed. By continuously monitoring the discharge process, the electrolyte remained colorless and transparent throughout, indicating the absence of soluble intermediate products and shuttling during the discharge process. Additionally, the self-discharge rate of the battery was tested (Fig. S6b). The Cu-SPAN/CNT battery was discharged to 1.80 V and then left to rest for 24 and 240 h before resuming discharge. No significant capacity decay was observed, which can be attributed to its unique solid-solid conversion mechanism. This mechanism limits the loss of active intermediate products but is also the cause of the sluggish electrochemical reaction kinetics. Therefore, the Cu_2S-Li_2S displacement reaction was introduced to accelerate the SPAN/Li_2S solid-solid conversion reaction.

The galvanostatic charge-discharge (GCD) test results at 1 C demonstrate that the initial reversible specific capacity of SPAN is only 1318 mAh g^{-1}, and the capacity drops sharply after 800 cycles, indicating battery failure. In contrast, Cu-SPAN/CNT exhibits a higher reversible specific capacity and sulfur utilization rate, initially delivering a specific capacity of 1450 mAh g^{-1}, and it maintains stability over 1000 cycles with minimal capacity decay, retaining 80.3 % of its capacity, which equates to an average decay of only 0.0197 % per cycle (Fig. 4a). At a higher C-rate of 2 C, SPAN exhibited a sharp decline in capacity after 780 cycles, with a mode of failure consistent with that at 1 C. Conversely, the Cu-SPAN/CNT, benefiting from enhanced electrochemical reaction kinetics, was able to stably cycle for 1000 cycles, with a capacity retention of 78 % after 800 cycles, demonstrating excellent long-term cycling stability (Fig. 4c). Comparing the voltage-capacity curves at 1 C, from 2nd to 800th cycle, the Cu-SPAN/CNT battery exhibited smaller capacity attenuation and polarization voltage growth relative to SPAN. The potential hysteresis gap of the SPAN increases from 0.59 V to 1.41 V, while that of the Cu-SPAN/CNT merely grows from 0.48 V to 0.89 V (Fig. 4b). In addition, at the 100th cycle of 1 C, the Cu-SPAN/CNT demonstrates an excellent energy utilization efficiency of 79.8 %, while the efficiency of SPAN is 77.4 %. After 800 cycles, the energy utilization efficiencies of Cu-SPAN/CNT and SPAN are 70.5 % and 65.3 % respectively, and the gap further increases from 2.4 % to 5.2 %, which indicates that the energy loss becomes more severe with the progress of cycling (Fig. S7).These results indicate that the addition of CNT and the Cu_2S-Li_2S displacement reaction can effectively improve the redox kinetics and reduce cycling polarization. On the one hand, enhanced redox kinetics can reduce the occurrence of side reactions and then improve the long-term cycling performance. On the other hand, the reduced polarization voltage contributes to the improvement of energy utilization efficiency, which is significant for saving energy loss in large-scale energy storage. To compare the stability of SPAN and Cu-SPAN/CNT at different current densities, C-rate performance tests were conducted at 0.2C–4 C. As shown in Fig. 4d, the reversible specific capacities of SPAN at 0.2 C, 0.5 C, 1 C, 2 C, 3 C, and 4 C rates were 1424, 1400, 1354, 1266, 1187, and 1078 mAh g^{-1}, respectively. In contrast, the reversible specific capacities of Cu-SPAN/CNT were 1456, 1414, 1372, 1304, 1255, and 1207 mAh g^{-1}, all of which were higher than those of SPAN, indicating a higher sulfur utilization rate. Additionally, by comparing the voltage-specific capacity curves at different C-rates (Fig. S8b–c), Cu-SPAN/CNT exhibits smaller polarization. Consequently, Cu-SPAN/CNT maintains a high specific capacity exceeding 1200 mAh g^{-1} even at a high rate of 4 C, which amounts to approximately 83 % of the capacity at 0.2C. When the current density is reduced back to 0.2 C, Cu-SPAN/CNT can still deliver a specific capacity of 1439 mAh g^{-1}, nearly equivalent to its initial value, demonstrating the excellent electrochemical stability and high sulfur utilization rate of Cu-SPAN/CNT.

To assess sulfur utilization and the improvement effects on kinetics under high SPAN loading, GCD tests were conducted, with the results depicted in Fig. 4e. Even at an ultra-high SPAN loading of 15.28 mg cm^{-2} (6.75 mg cm^{-2} of Sulfur), Cu-SPAN/CNT demonstrates cycling stability. At a rate of 0.2C, Cu-SPAN/CNT delivers a reversible specific capacity of 1378 mAh g^{-1}, corresponding to a reversible areal capacity as high as 9.3 mAh cm^{-2}, with a very high sulfur utilization rate of approximately 82.4 % (Fig. S8d). This indicates that the construction of excellent conductive network with Cu as the metal active center helps to

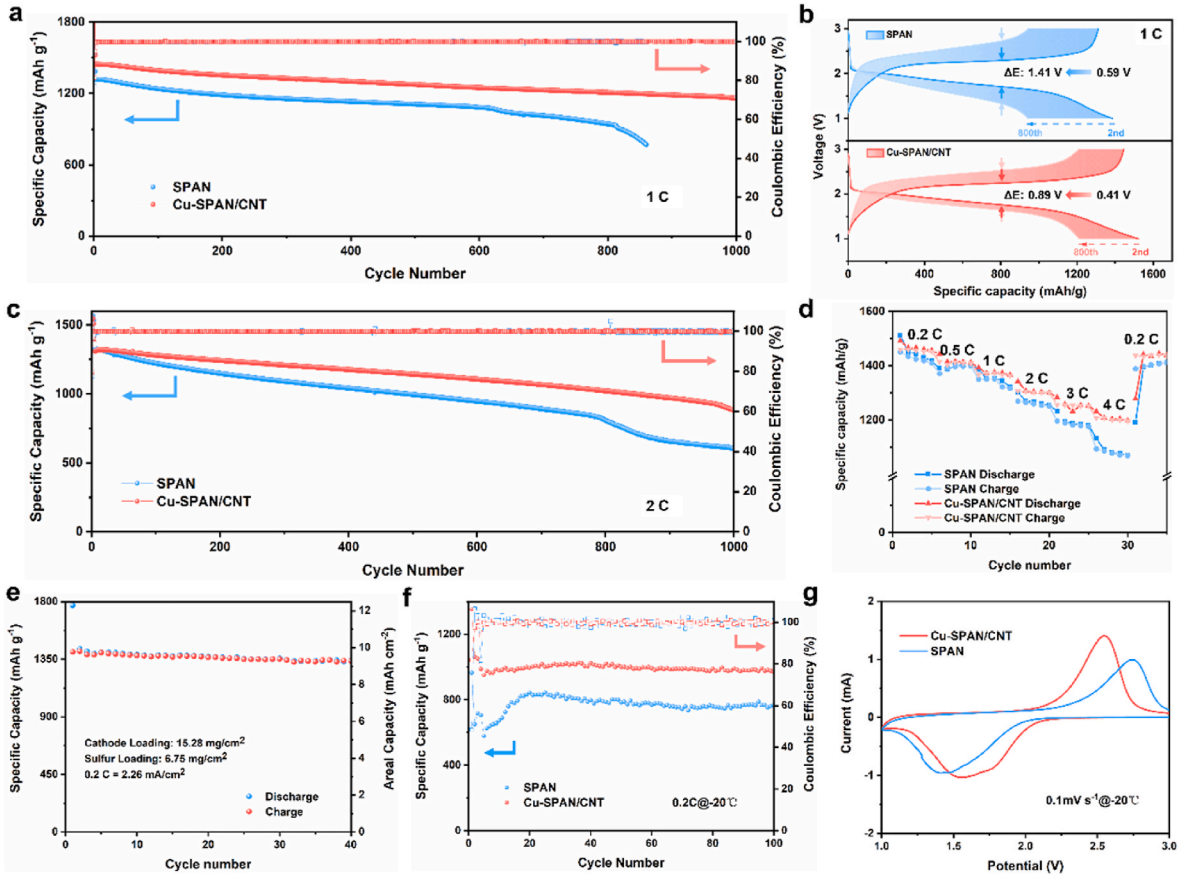

Fig. 4. (a, c) The cycling performance of SPAN and Cu-SPAN/CNT at (a) 1C (c) 2 C. (b) GCD profiles of SPAN and Cu-SPAN/CNT at 1 C from the 2nd to the 800th cycle. (d) C-rate capabilities of SPAN and Cu-SPAN/CNT. (e) The cycling performance of high loading Cu-SPAN/CNT cathode. (f) The cycling performance and (g) CV curves of SPAN and Cu-SPAN/CNT at −20 °C.

enhance the kinetics of SPAN, fully leveraging the high-capacity advantage of SPAN under high loading. Under low-temperature conditions, the internal kinetic processes of batteries are typically hindered, preventing SPAN from fully participating in electrochemical reactions, which in turn fail to fully exploit capacity. To evaluate the improvement in kinetic reaction performance under low-temperature conditions, GCD tests were conducted at −20 °C (Fig. 4f). Compared to the SPAN, which offers a reversible specific capacity of only around 800 mAh g^{-1}, Cu-SPAN/CNT can deliver a high specific capacity of approximately 1000 mAh g^{-1}, corresponding to sulfur utilization rates of 47.8 % and 59.8 %, respectively. At the beginning of cycling, both SPAN and Cu-SPAN/CNT undergo an "activation" process, where the specific capacity gradually increases over the first few cycles, a phenomenon commonly observed in low-temperature cycling[42–44]. However, the "activation" process for Cu-SPAN/CNT is significantly shorter than that for SPAN, with the battery reaching a stable state after only 5 cycles, whereas SPAN requires 20 cycles (Fig. S8e–f). Simultaneously, compared to SPAN, Cu-SPAN/CNT exhibits a larger and more extended voltage plateau, as well as a lower activation potential for Li_2S. The charging voltage plateaus are 2.75 V and 2.45 V, respectively, showing a significant difference. Additionally, CV tests conducted at −20 °C characterized the "activation" process, further investigating the differences in electrochemical kinetics at low temperature (Fig. 4g). The results reveal that the CV curves at −20 °C are like those (Fig. 2f) at room temperature (RT), but due to the sluggish redox kinetics at low temperature, the potential gap between the oxidation and reduction peaks is wider compared to that at RT, indicating greater electrochemical polarization of the battery. Owing to the CNT and the rapid Cu_2S-Li_2S displacement reaction, Cu-SPAN/CNT exhibits larger peak currents for both oxidation and reduction, and a smaller potential difference between the redox peaks (0.99 V in contrast to 1.35 V), showing a significant improvement over SPAN.

To investigate the mechanism of the displacement of Cu_2S-Li_2S, *in situ* XRD tests were carried out, the schematic diagram of which is shown in Fig. 5a. As the Cu-SPAN/CNT discharges from 3.0 V to 1.0 V, the characteristic peak of Li_2S [27] reduction product in SPAN at 27.0° (PDF #077–2145) gradually forms and reaches its maximum, and as the Cu-SPAN/CNT charges back to 3.0 V, this characteristic peak disappears, confirming that the discharge product of SPAN is Li_2S [9,10,26]. Concurrently, the intensity changes of the Cu characteristic peak at 43.3° (PDF #085–1326) exhibit an initial increase followed by a decrease [37], indicating that the valence changes of Cu are in line with the mutual conversion of the SPAN/Li_2S redox couple (Fig. 5b–c). The presence of Cu_2S lattice fringes in the TEM of the cycled Cu-SPAN/CNT cathode (Fig. 1f) further substantiates that Cu participates in the battery's redox reactions in the form of Cu/Cu_2S [38]. XPS measurement results corroborate the conclusions (Fig. 5d). With increasing depth of discharge, the S 2p spectra of Cu-SPAN/CNT at 0 % DOD, 50 % DOD, and 100 % DOD demonstrate a gradual transition from C-S_x (163.3 and 164.5 eV) to Li-S (161.4 and 162.6 eV) [45,46], while the Cu-S (161.6 and 162.8 eV) [47] peak gradually diminish and eventually disappear. Upon recharging the battery to 50 % SOC, the Li-S peaks weaken and the C-S_x and Cu-S intensities enhance, indicating that the Cu/Cu_2S participation in the SPAN/Li_2S reaction is reversible. Therefore, experimental characterization reveals Cu/Cu_2S optimizes SPAN cathodes through: (1) synergistic conductivity enhancement with CNT; (2) introducing a rapid, reversible Cu_2S-Li_2S displacement reaction to activate decomposition kinetics and improve SPAN's cycling energy efficiency.

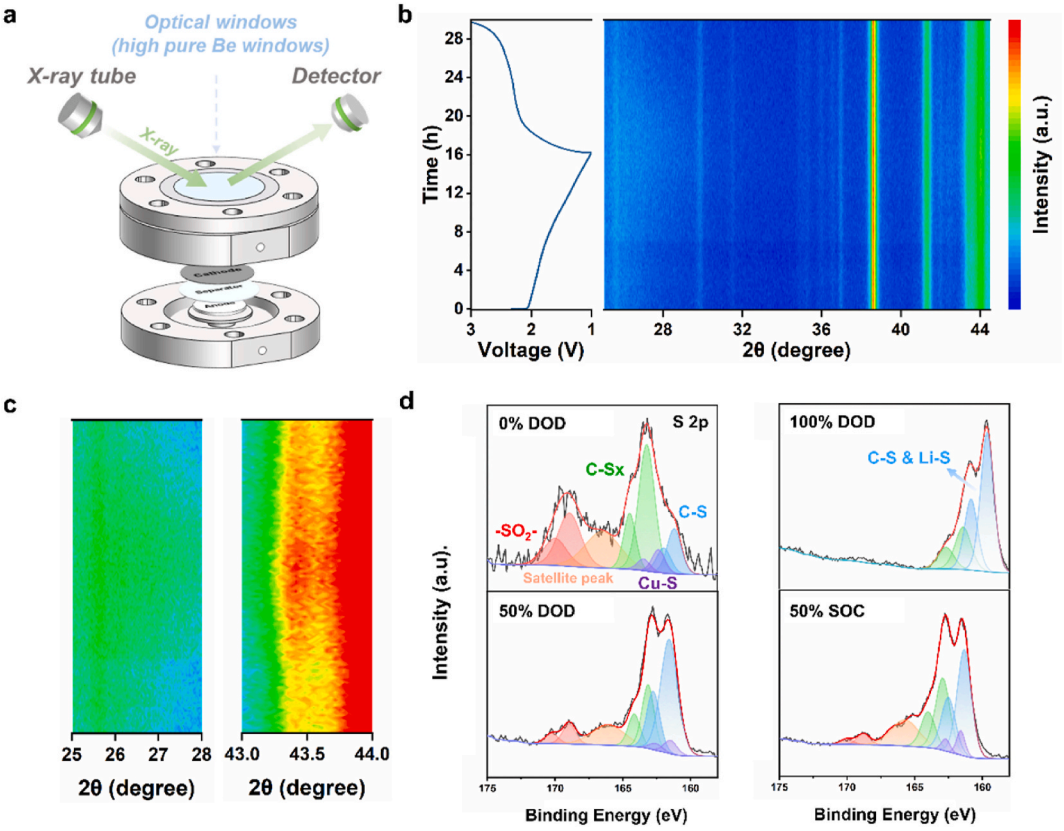

Fig. 5. (a) Schematic diagram of battery for *in situ* XRD test. (b, c) *in situ* XRD spectra of Cu-SPAN/CNT battery. (d) XPS spectra of S 2p in the cycled Cu-SPAN/CNT cathodes of different DOD & SOC.

4. Conclusion

In this study, the Cu-SPAN/CNT cathode was successfully fabricated, where Cu serves as the active center. Concurrently, the fast and reversible displacement reaction of Cu_2S-Li_2S was introduced into the redox reaction of SPAN. Along with the introduction of the displacement reaction and the synergistic rapid conduction of CNT, the process enhanced the conversion rate of SPAN/Li_2S, improved the sulfur utilization efficiency, and strengthened the electrochemical reaction kinetics. Enhanced redox kinetics can reduce the occurrence of side reactions and then improve long-cycle-life and energy utilization efficiency. Therefore, Cu-SPAN/CNT exhibits a high-capacity retention of 80.3 % after 1000 cycles at 1 C and demonstrates superior performance under a high C-rate of 4 C, high loading, and a low temperature of −20 °C, reducing the useless energy loss during cycling and achieving excellent energy utilization efficiency. In summary, taking the SPAN-Li battery as an example, this study provides a simple electrode engineering strategy for enhancing electrochemical reaction kinetics and constructing energy storage batteries with high energy utilization efficiency.

CRediT authorship contribution statement

Yi Deng: Writing – original draft, Software, Methodology, Investigation, Formal analysis, Data curation, Conceptualization. **Qichen Chen:** Writing – review & editing, Data curation. **Jiaxiang Liu:** Writing – review & editing, Data curation. **Yuejing Zeng:** Writing – review & editing, Data curation. **Ruilai Ye:** Data curation. **Xinyu Li:** Data curation. **Peng Zhang:** Writing – review & editing, Supervision, Project administration, Funding acquisition. **Jinbao Zhao:** Writing – review & editing, Supervision, Project administration, Funding acquisition.

Declaration of competing interest

The authors declare that they have no known competing financial interests or personal relationships that could have appeared to influence the work reported in this paper.

Acknowledgments

This work is supported by the National Key Research and Development Program of China (Grant No. 2021YFB2400300), the National Natural Science Foundation of China (Grant No. 21875195). We also would like to express gratitude for the support of Tan Kah Kee Innovation Laboratory.

Appendix A. Supplementary data

Supplementary data to this article can be found online at https://doi.org/10.1016/j.jpowsour.2025.237989.

Data availability

Data will be made available on request.

References

[1] X. Chen, L. Peng, L. Wang, J. Yang, Z. Hao, J. Xiang, K. Yuan, Y. Huang, B. Shan, L. Yuan, J. Xie, Ether-compatible sulfurized polyacrylonitrile cathode with excellent performance enabled by fast kinetics via selenium doping, Nat. Commun. 10 (2019) 1021, https://doi.org/10.1038/s41467-019-08818-6.

[2] B. Huang, H. Hua, L. Peng, X. Wang, X. Shen, R. Li, P. Zhang, J. Zhao, The functional separator for lithium-ion batteries based on phosphonate modified nano-scale silica ceramic particles, J. Power Sources 498 (2021) 229908, https://doi.org/10.1016/j.jpowsour.2021.229908.

[3] X. Qiao, C. Wang, J. Zang, B. Guo, Y. Zheng, R. Zhang, J. Cui, X. Fang, Conductive inks composed of multicomponent carbon nanomaterials and hydrophilic polymer binders for high-energy-density lithium-sulfur batteries, Energy Storage Mater. 49 (2022) 236–245, https://doi.org/10.1016/j.ensm.2022.04.022.
[4] R. Liu, Z. Wei, L. Peng, L. Zhang, A. Zohar, R. Schoeppner, P. Wang, C. Wan, D. Zhu, H. Liu, Z. Wang, S.H. Tolbert, B. Dunn, Y. Huang, P. Sautet, X. Duan, Establishing reaction networks in the 16-electron sulfur reduction reaction, Nature 626 (2024) 98–104, https://doi.org/10.1038/s41586-023-06918-4.
[5] T. Hu, Y. Guo, Y. Meng, Z. Zhang, J. Yu, J. Cai, Z. Yang, Uniform lithium deposition induced by copper phthalocyanine additive for durable lithium anode in lithium-sulfur batteries, Chin. Chem. Lett. 35 (2024) 108603, https://doi.org/10.1016/j.cclet.2023.108603.
[6] Y. Wang, H. Chen, F. Yu, S. Wei, J. Song, Q. He, Y. Xie, M. Huang, C. Lu, Oxygen self-doping pyrolyzed polyacrylic acid as sulfur host with physical/chemical adsorption dual function for lithium-sulfur batteries, Chin. Chem. Lett. 35 (2024) 109001, https://doi.org/10.1016/j.cclet.2023.109001.
[7] H. Yang, A. Naveed, Q. Li, C. Guo, J. Chen, J. Lei, J. Yang, Y. Nuli, J. Wang, Lithium sulfur batteries with compatible electrolyte both for stable cathode and dendrite-free anode, Energy Storage Mater. 15 (2018) 299–307, https://doi.org/10.1016/j.ensm.2018.05.014.
[8] W. Zuo, Y. Guo, C. Zhang, L. Zhang, S. Zhang, Mussel and cobweb inspired high areal capacity SPAN electrode, Small 20 (2024) 2309126, https://doi.org/10.1002/smll.202309126.
[9] W. Wang, Z. Cao, G.A. Elia, Y. Wu, W. Wahyudi, E. Abou-Hamad, A.-H. Emwas, L. Cavallo, L.-J. Li, J. Ming, Recognizing the mechanism of sulfurized polyacrylonitrile cathode materials for Li–S batteries and beyond in Al–S batteries, ACS Energy Lett. 3 (2018) 2899–2907, https://doi.org/10.1021/acsenergylett.8b01945.
[10] J. Liu, H. Lu, Q. Wang, X. Kong, C. Hao, J. Yang, Y. NuLi, H. Duan, J. Wang, Roles of the polymer backbone for sulfurized polyacrylonitrile cathodes in rechargeable lithium batteries, J. Am. Chem. Soc. 147 (2024) 426–435, https://doi.org/10.1021/jacs.4c11216.
[11] Q. Wu, F. Ma, W. Zhang, H. Yan, X. Chen, S. Cheng, J. Xie, Bifunctional Li $_2$ Se mediator to accelerate sulfur conversion and lithium deposition kinetics in lithium–sulfurized polyacrylonitrile batteries, ACS Appl. Energy Mater. 6 (2023) 7138–7146, https://doi.org/10.1021/acsaem.3c00815.
[12] C. Zhao, W. Chen, M. Zhao, Y. Song, J. Liu, B. Li, T. Yuan, C. Chen, Q. Zhang, J. Huang, Redox mediator assists electron transfer in lithium–sulfur batteries with sulfurized polyacrylonitrile cathodes, Ecomat 3 (2021) e12066, https://doi.org/10.1002/eom2.12066.
[13] L. Wang, H. Shi, Y. Xie, Z. Wu, Boosting solid–solid conversion kinetics of sulfurized polyacrylonitrile via MoS $_2$ doping for high-rate and long-life Li-S batteries, Carbon Neutralization 2 (2023) 262–270, https://doi.org/10.1002/cnl2.61.
[14] Wei Zhang, F. Ma, Q. Wu, Z. Cai, W. Zhong, Z. Zeng, S. Cheng, J. Xie, Bifunctional fluorinated anthraquinone additive for improving kinetics and interfacial chemistry in rechargeable Li–S batteries, ACS Appl. Energy Mater. 5 (2022) 15719–15728, https://doi.org/10.1021/acsaem.2c03306.
[15] S. Wang, B. Lu, D. Cheng, Z. Wu, S. Feng, M. Zhang, W. Li, Q. Miao, M. Patel, J. Feng, E. Hopkins, J. Zhou, S. Parab, B. Bhamwala, B. Liaw, Y.S. Meng, P. Liu, Structural transformation in a sulfurized polymer cathode to enable long-life rechargeable lithium–sulfur batteries, J. Am. Chem. Soc. 145 (2023) 9624–9633, https://doi.org/10.1021/jacs.3c00628.
[16] L. Yin, J. Wang, J. Yang, Y. Nuli, A novel pyrolyzed polyacrylonitrile-sulfur@MWCNT composite cathode material for high-rate rechargeable lithium/sulfur batteries, J. Mater. Chem. 21 (2011) 6807–6810, https://doi.org/10.1039/C1JM00047K.
[17] L. Yin, J. Wang, F. Lin, J. Yang, Y. Nuli, Polyacrylonitrile/graphene composite as a precursor to a sulfur-based cathode material for high-rate rechargeable Li–S batteries, Energy Environ. Sci. 5 (2012) 6966–6972, https://doi.org/10.1039/C2EE03495F.
[18] Y. Liu, A.K. Haridas, Y. Lee, K.-K. Cho, J.-H. Ahn, Freestanding porous sulfurized polyacrylonitrile fiber as a cathode material for advanced lithium sulfur batteries, Appl. Surf. Sci. 472 (2019) 135–142, https://doi.org/10.1016/j.apsusc.2018.03.062.
[19] X. Hu, H. Jiang, Q. Hou, M. Yu, X. Jiang, G. He, X. Li, Scalable SPAN membrane cathode with high conductivity and hierarchically porous framework for enhanced ion transfer and cycling stability in Li–S batteries, ACS Mater. Lett. 5 (2023) 2047–2057, https://doi.org/10.1021/acsmaterialslett.3c00450.
[20] S. Li, Z. Han, W. Hu, L. Peng, J. Yang, L. Wang, Y. Zhang, B. Shan, J. Xie, Manipulating kinetics of sulfurized polyacrylonitrile with tellurium as eutectic accelerator to prevent polysulfide dissolution in lithium-sulfur battery under dissolution-deposition mechanism, Nano Energy 60 (2019) 153–161, https://doi.org/10.1016/j.nanoen.2019.03.023.
[21] S. Ma, Z. Zhang, Y. Wang, Z. Yu, C. Cui, M. He, H. Huo, G. Yin, P. Zuo, Iodine-doped sulfurized polyacrylonitrile with enhanced electrochemical performance for lithium sulfur batteries in carbonate electrolyte, Chem. Eng. J. 418 (2021) 129410, https://doi.org/10.1016/j.cej.2021.129410.
[22] Y. Hu, B. Li, X. Jiao, C. Zhang, X. Dai, J. Song, Stable cycling of phosphorus anode for sodium-ion batteries through chemical bonding with sulfurized polyacrylonitrile, Adv. Funct. Mater. 28 (2018) 1801010, https://doi.org/10.1002/adfm.201801010.
[23] H. Li, W. Xue, L. Wang, T. Liu, Two competing reactions of sulfurized polyacrylonitrile produce high-performance lithium–sulfur batteries, ACS Appl. Mater. Interfaces 13 (2021) 25002–25009, https://doi.org/10.1021/acsami.1c06004.
[24] M. Roucan, M. Kielmann, S.J. Connon, S.S.R. Bernhard, M.O. Senge, Conformational control of nonplanar free base porphyrins: towards bifunctional catalysts of tunable basicity, Chem. Commun. 54 (2018) 26–29, https://doi.org/10.1039/C7CC08099A.
[25] A. Abdul Razzaq, G. Chen, X. Zhao, X. Yuan, J. Hu, Z. Li, Y. Chen, J. Xu, R. Shah, J. Zhong, Y. Peng, Z. Deng, Cobalt coordination with pyridines in sulfurized polyacrylonitrile cathodes to form conductive pathways and catalytic M-N4S sites for accelerated Li-S kinetics, J. Energy Chem. 61 (2021) 170–178, https://doi.org/10.1016/j.jechem.2021.01.012.
[26] X. Wang, Y. Qian, L. Wang, H. Yang, H. Li, Y. Zhao, T. Liu, Sulfurized polyacrylonitrile cathodes with high compatibility in both ether and carbonate electrolytes for ultrastable lithium–sulfur batteries, Adv. Funct. Mater. 29 (2019) 1902929, https://doi.org/10.1002/adfm.201902929.
[27] H. Liu, Y. Zhang, Y. Li, N. Han, H. Liu, X. Zhang, Solid-state transformations of active materials in the pores of sulfurized-polyacrylonitrile fiber membranes via nucleophilic reactions for high-loading and free-standing lithium–sulfur battery cathodes, Adv. Fiber Mater. 6 (2024) 772–785, https://doi.org/10.1007/s42765-024-00391-y.
[28] J. Li, K. Li, M. Li, D. Gosselink, Y. Zhang, P. Chen, A sulfur–polyacrylonitrile/graphene composite cathode for lithium batteries with excellent cyclability, J. Power Sources 252 (2014) 107–112, https://doi.org/10.1016/j.jpowsour.2013.11.088.
[29] R. He, Y. Li, S. Wei, H. Liu, S. Zhang, N. Han, H. Liu, X. Wang, X. Zhang, Construction of high-performance sulfurized poly(acrylonitrile) cathodes for lithium-sulfur batteries via catalytic and conductive regulation, J. Alloys Compd. 919 (2022) 165838, https://doi.org/10.1016/j.jallcom.2022.165838.
[30] W. Xue, W. Xu, W. Wang, G. Gao, L. Wang, Iodine-doped fibrous sulfurized polyacrylonitrile with accelerated reaction kinetics, Compos. Commun. 30 (2022) 101078, https://doi.org/10.1016/j.coco.2022.101078.
[31] Q. Wu, W. Zhang, S. Li, W. Zhong, H. Zhu, Z. Zeng, C. Yu, S. Cheng, J. Xie, Electrospun sulfurized polyacrylonitrile nanofibers for long-term cycling stability and high-rate lithium–sulfur batteries, ACS Appl. Energy Mater. 5 (2022) 5212–5218, https://doi.org/10.1021/acsaem.2c00585.
[32] K. Wang, T. Zhao, Y. Liu, T. Yu, G. Chen, W. Tang, L. Li, F. Wu, R. Chen, Accelerating redox kinetics of sulfurized polyacrylonitrile nanosheets by trace doping of element, Chem. Eng. J. 487 (2024) 150300, https://doi.org/10.1016/j.cej.2024.150300.
[33] Q. Fan, B. Li, Y. Si, Y. Fu, Lowering the charge overpotential of Li_2 S *via* the inductive effect of phenyl diselenide in Li–S batteries, Chem. Commun. 55 (2019) 7655–7658, https://doi.org/10.1039/C8CC09565E.
[34] X. Zhang, J. Li, C. Gao, C. Shi, L. He, Q. Xiang, B. Hong, Y. Lai, Z. Zhang, K. Zhang, Promoting the conversion of Li2S by functional additives phenyl diselenide in lithium–sulfur batteries, J. Power Sources 482 (2021) 228967, https://doi.org/10.1016/j.jpowsour.2020.228967.
[35] A. Débart, L. Dupont, R. Patrice, J.-M. Tarascon, Reactivity of transition metal (Co, Ni, Cu) sulphides versus lithium: the intriguing case of the copper sulphide, Solid State Sci. 8 (2006) 640–651, https://doi.org/10.1016/j.solidstatesciences.2006.01.013.
[36] M.T. McDowell, Z. Lu, K.J. Koski, J.H. Yu, G. Zheng, Y. Cui, In situ observation of divergent phase transformations in individual sulfide nanocrystals, Nano Lett. 15 (2015) 1264–1271, https://doi.org/10.1021/nl504436m.
[37] Y. Wang, X. Feng, Y. Xiong, S. Stoupin, R. Huang, M. Zhao, M. Xu, P. Zhang, J. Zhao, H.D. Abruña, An innovative lithium ion battery system based on a Cu2S anode material, ACS Appl. Mater. Interfaces 12 (2020) 17396–17405, https://doi.org/10.1021/acsami.9b21982.
[38] L. Tan, A. Li, Y. Yang, J. Zhang, X. Niu, N. Li, L. Liu, L. Guo, Y. Zhu, Highly active and stable Li_2S−Cu nanocomposite cathodes enabled by kinetically favored displacement interconversion between Cu_2S and Li_2S, Angew. Chem. Int. Ed. 61 (2022) e202206012, https://doi.org/10.1002/anie.202206012.
[39] J. Wang, J. Yang, J. Xie, N. Xu, A novel conductive polymer-sulfur composite cathode material for rechargeable lithium batteries, Adv. Mater. 14 (2002) 963–965, https://doi.org/10.1002/1521-4095(20020705)14:13/14<963::AID-ADMA963>3.0.CO;2-P.
[40] J. Wang, J. Yang, C. Wan, K. Du, J. Xie, N. Xu, Sulfur composite cathode materials for rechargeable lithium batteries, Adv. Funct. Mater. 13 (2003) 487–492, https://doi.org/10.1002/adfm.200304284.
[41] J. Qin, Y. Lu, R. Wang, Z. Li, T. Shen, D. Wang, Sulfurization accelerator coupled Fe1−xS electrocatalyst boosting SPAN cathode performance, Nano Res. 16 (2023) 9231–9239, https://doi.org/10.1007/s12274-023-5573-6.
[42] S. Tan, H. Liu, Z. Wu, C. Weiland, S.-M. Bak, A. Ronne, P. Liu, M.S. Whittingham, Z. Shadike, E. Hu, X.-Q. Yang, Isoxazole-based electrolytes for lithium metal protection and lithium-sulfurized polyacrylonitrile (SPAN) battery operating at low temperature, J. Electrochem. Soc. 169 (2022) 30513, https://doi.org/10.1149/1945-7111/ac58c5.
[43] D. Guo, S. Thomas, J.K. El-Demellawi, Z. Shi, Z. Zhao, C.G. Canlas, Y. Lei, J. Yin, Y. Zhang, M.N. Hedhili, M. Arsalan, Y. Zhu, O.M. Bakr, O.F. Mohammed, H. N. Alshareef, Electrolyte engineering for thermally stable Li–S batteries operating from −20 °C to 100 °C, Energy Environ. Sci. 17 (2024) 8151–8161, https://doi.org/10.1039/D4EE03191A.
[44] J. Wu, M. Li, L. Ma, X. Li, X. Chen, J. Long, Y. Wang, X. Li, J. Liu, Z. Guo, Y. Chen, Engineering densely packed ion-cluster electrolytes for wide-temperature lithium–sulfurized polyacrylonitrile batteries, ACS Nano 18 (2024) 32984–32994, https://doi.org/10.1021/acsnano.4c13280.
[45] Z.-Q. Jin, Y.-G. Liu, W.-K. Wang, A.-B. Wang, B.-W. Hu, M. Shen, T. Gao, P.-C. Zhao, Y.-S. Yang, A new insight into the lithium storage mechanism of sulfurized

polyacrylonitrile with no soluble intermediates, Energy Storage Mater. 14 (2018) 272–278, https://doi.org/10.1016/j.ensm.2018.04.013.
[46] M.A. Weret, C.-F. Jeffrey Kuo, T.S. Zeleke, T.T. Beyene, M.-C. Tsai, C.-J. Huang, G. B. Berhe, W.-N. Su, B.-J. Hwang, Mechanistic understanding of the sulfurized-poly (acrylonitrile) cathode for lithium-sulfur batteries, Energy Storage Mater. 26 (2020) 483–493, https://doi.org/10.1016/j.ensm.2019.11.022.
[47] R. Zhang, C. Cui, R. Xiao, R. Li, T. Mu, H. Huo, Y. Ma, G. Yin, P. Zuo, Interface regulation of Mg anode and redox couple conversion in cathode by copper for high-performance Mg-S battery, Chem. Eng. J. 451 (2023) 138663, https://doi.org/10.1016/j.cej.2022.138663.